Raman Spectra of Bismuth Germanium Oxide and Bismuth Silicon Oxide*

S. Venugopalan and A. K. Ramdas
Department of Physics, Purdue University, Lafayette, Indiana 47907
(Received 10 January 1972)

Raman spectra of single crystals of bismuth germanium oxide ($Bi_{12}GeO_{20}$) and bismuth silicon oxide ($Bi_{12}SiO_{20}$) are studied at 300, 77, and 15 °K. These crystals are isomorphous, exhibit optical activity, and belong to the cubic space group $T^3(I23)$. On the basis of one formula unit per primitive cell, a group-theoretical analysis predicts $8A$ (totally symmetric), $8E$ (doubly degenerate), and $24F$ (triply degenerate) zone-center optical phonons, without taking into account the LO-TO splitting of the polar F modes. Phonons belonging to all three symmetries are Raman active. The most detailed spectra with well-resolved lines are observed in both crystals at 15 °K. The spectrum of $Bi_{12}GeO_{20}$ at 15 °K consists of a total of 36 lines which lie in the region 40–720 cm^{-1}. A total of 43 lines in the region 40–850 cm^{-1} are observed in $Bi_{12}SiO_{20}$ at 15 °K. The polarization of the Raman lines in both crystals is studied at 15 °K for the following two crystalline orientations: one with {100} faces and the other with (100), (011), and $(0\bar{1}1)$ faces. Both right-angle and back-scattering geometries were used in polarization studies, and all the observed lines have been classified according to the irreducible representations of the point group T. Some of the F modes in each crystal show LO-TO splitting. With plane-polarized radiation incident along [100] and scattered along [010] or [011], the intensity oscillations of prominent lines of $Bi_{12}GeO_{20}$ are studied as a function of the angle between the electric vector of the incident radiation and the scattering plane. The observed intensity oscillations for the lines studied in this manner lead to symmetry assignments which are in agreement with those determined from polarization studies. In view of the fact that there exist tightly bound groups of MO_4 units in these crystals, where $M \equiv$ Ge or Si, a possible approach towards correlating some of the observed lines as originating from the normal modes of the MO_4 unit is suggested.

I. INTRODUCTION

Bismuth germanium oxide ($Bi_{12}GeO_{20}$) and bismuth silicon oxide ($Bi_{12}SiO_{20}$) have been recently grown as large single crystals.[1,2] These are isomorphous, possess the $T(23)$ point-group symmetry, and belong to the space group $T^3(I23)$.[2,3] As expected for crystals of this symmetry, both exhibit isotropic optical activity.[4,5] The optical rotatory power and its dispersion are remarkably large for these crystals. For example, the rotatory power at ~5893 Å is ~25°/mm for both the crystals; this is to be compared with 3.13°/mm at the same wavelength, for sodium chlorate, a well-known crystal of the same point-group symmetry.[6]

Consistent with their symmetry, both bismuth germanium oxide and bismuth silicon oxide may be piezoelectric. Indeed, bismuth germanium oxide has been shown to be strongly piezoelectric,[7] the piezoelectric coefficient $d_{14} = 8.5 \times 10^{-7}$ statcoulomb/dyn being nearly an order of magnitude larger than that of zinc blende.[8] It is also of interest to note that the electro-optic coefficient $N_0^3 r_{41}$ has a fairly high value[4] of 5×10^{-9} cm/V which is comparable to that of zinc blende.[9] Thus both $Bi_{12}GeO_{20}$ and $Bi_{12}SiO_{20}$ are of considerable interest in view of their unusual optical and electro-optical properties. In this paper we present results of a Raman-scattering study of the lattice vibrations of these crystals.[10]

II. EXPERIMENTAL PROCEDURE

$Bi_{12}GeO_{20}$ and $Bi_{12}SiO_{20}$ single-crystal ingots of high optical quality were obtained from Isomet Corp.[11] They were oriented using x rays, and samples with the following two orientations were obtained: one with {100} faces and the other with (100), (011), and $(0\bar{1}1)$ faces. For back-scattering measurements, a thin slice with {100} faces was used. After cutting, the crystals were ground with successively finer grade Carborundum powders and finally polished on AB Microcloth polishing cloth with 1-μ diamond paste, using Metadi oil as lubricant.[12] $Bi_{12}GeO_{20}$ crystals grown in our laboratory by Louise Roth were also examined and the spectra were identical to those obtained from the commercial crystals.

In the present studies the 6328-Å radiation from a Spectra-Physics (model 125) He-Ne laser[13] and the 5145- and 4880-Å radiations from a Coherent Radiation (model 52A) Ar^+ laser[14] were used. The onset of strong absorption for both $Bi_{12}GeO_{20}$[1,4] and $Bi_{12}SiO_{20}$[2] occurs around 5000 Å and extends toward shorter wavelengths. Thus the lines of the Ar^+ laser are strongly absorbed by these crystals, and they suffered damage if excessive power levels were used. In contrast, the crystals are highly transparent at 6328 Å and beyond. In addition, it should be noted that the optical rotatory power at 5000 Å[4,5] is ~43°/mm in contrast to 22°/mm at 6328 Å.

Hence, for polarization measurements excitation with 6328 Å proves to be somewhat more advantageous. Most of the measurements made during the present investigation were performed with the 6328-Å radiation with ~ 50 mW of incident power. The 5145- and 4880-Å radiations from the Ar^+ laser, with power levels ~ 100 mW, were used to ensure that the observed spectra were due to Raman scattering; in this context, the anti-Stokes spectra were also recorded.

Light scattered from the sample was focused on the entrance slit of a Jarrell-Ash double monochromator (model 25-100)[15] of 1-m focal length and equipped with gratings having 1180 grooves/mm and blazed at 5000 Å. A cooled ITT FW 130 photomultiplier tube[16] was used as the detector together with a photon counting assembly.[17] The spectral resolution used in the measurements reported here is in the range 1–1.5 cm^{-1}. Line positions are accurate to ± 0.5 cm^{-1} for most lines and within ± 1.0 cm^{-1} for the broad weaker lines. The crystals were mounted on the cold finger of a three-window optical cryostat[18] to facilitate low-temperature measurements. A Spectra-Physics (model 310) polarization rotator was used for rotating the polarization of incident light in polarization measurements or measurement of intensity oscillations of a given line. The latter technique is discussed in detail in Sec. III. Circular polarization of incident light was generated using a Babinet-Soleil compensator,[19] set as a quarter-wave plate at 6328 Å.

As noted earlier, the optical rotatory power is rather large in both $Bi_{12}GeO_{20}$ and $Bi_{12}SiO_{20}$. Even at 6328 Å, the rotatory power of 22°/mm can scramble polarization features unless due care is exercised in this regard. Raman spectra of optically active crystals of high symmetry have been studied in the past, using lasers.[20–22] Optical activity can be circumvented when the crystal symmetry is not cubic and ignored when its magnitude is not large. In the present study, however, owing both to its isotropic nature and large magnitude, optical activity could not be neglected. To minimize its effects, therefore, scattered radiation from only the first 1 mm of the laser beam through the crystal was sampled, the scattering face being masked off along the remaining length. In addition, the laser beam entered the crystal within a depth of 1 mm from the scattering face. For back-scattering experiments, crystals of thickness from 1.0–2.0 mm were used.

TABLE I. Polarizability tensors for the A, E, and F zone-center phonons.

Symmetry	$X \parallel [100]$, $Y \parallel [010]$, $Z \parallel [001]$	$X \parallel [100]$, $Y' \parallel [011]$, $Z' \parallel [0\bar{1}1]$
A	$\begin{bmatrix} a & 0 & 0 \\ 0 & a & 0 \\ 0 & 0 & a \end{bmatrix}$	$\begin{bmatrix} a & 0 & 0 \\ 0 & a & 0 \\ 0 & 0 & a \end{bmatrix}$
E	$\mathcal{E}_E \begin{bmatrix} -1 & 0 & 0 \\ 0 & -1 & 0 \\ 0 & 0 & 2 \end{bmatrix}$, $\mathcal{E}_E \begin{bmatrix} \sqrt{3} & 0 & 0 \\ 0 & -\sqrt{3} & 0 \\ 0 & 0 & 0 \end{bmatrix}$	$\mathcal{E}_E \begin{bmatrix} -1 & 0 & 0 \\ 0 & \frac{1}{2} & \frac{3}{2} \\ 0 & \frac{3}{2} & \frac{1}{2} \end{bmatrix}$, $\mathcal{E}_E \begin{bmatrix} \sqrt{3} & 0 & 0 \\ 0 & -\frac{1}{2}\sqrt{3} & \frac{1}{2}\sqrt{3} \\ 0 & \frac{1}{2}\sqrt{3} & -\frac{1}{2}\sqrt{3} \end{bmatrix}$
F	$(X)\colon \mathcal{E}_F \begin{bmatrix} 0 & 0 & 0 \\ 0 & 0 & 1 \\ 0 & 1 & 0 \end{bmatrix}$, $(Y)\colon \mathcal{E}_F \begin{bmatrix} 0 & 0 & 1 \\ 0 & 0 & 0 \\ 1 & 0 & 0 \end{bmatrix}$, $(Z)\colon \mathcal{E}_F \begin{bmatrix} 0 & 1 & 0 \\ 1 & 0 & 0 \\ 0 & 0 & 0 \end{bmatrix}$	$\mathcal{E}_F \begin{bmatrix} 0 & 0 & 0 \\ 0 & 1 & 0 \\ 0 & 0 & -1 \end{bmatrix}$, $\mathcal{E}_F \begin{bmatrix} 0 & 1/\sqrt{2} & 1/\sqrt{2} \\ 1/\sqrt{2} & 0 & 0 \\ 1/\sqrt{2} & 0 & 0 \end{bmatrix}$, $\mathcal{E}_F \begin{bmatrix} 0 & 1/\sqrt{2} & -1/\sqrt{2} \\ 1/\sqrt{2} & 0 & 0 \\ -1/\sqrt{2} & 0 & 0 \end{bmatrix}$

III. THEORY

It is well known[23] that wave-vector conservation in a scattering process restricts the first-order (one-phonon) Raman effect in crystals to the zone-center optical phonons. In the same fashion, second- and higher-order (multiphonon) processes in-

TABLE II. Polarizability tensors for the LO-TO-split F zone-center phonons. The phonon polarizations are indicated in parentheses for right-angle scattering geometry with light incident along [100] direction and scattered along [010] or [011].

Symmetry	$X \parallel [100]$, $Y \parallel [010]$, $Z \parallel [001]$	$X \parallel [100]$, $Y' \parallel [011]$, $Z' \parallel [0\bar{1}1]$
$F(\mathrm{LO})$	$\mathcal{E}_F \begin{bmatrix} 0 & 0 & -1/\sqrt{2} \\ 0 & 0 & 1/\sqrt{2} \\ -1/\sqrt{2} & 1/\sqrt{2} & 0 \end{bmatrix}$	$\mathcal{E}_F \begin{bmatrix} 0 & -1/\sqrt{2} & 0 \\ -1/\sqrt{2} & 1/\sqrt{2} & 0 \\ 0 & 0 & -1/\sqrt{2} \end{bmatrix}$
$F(\mathrm{TO})_1$	$\mathcal{E}_F \begin{bmatrix} 0 & 0 & 1/\sqrt{2} \\ 0 & 0 & 1/\sqrt{2} \\ 1/\sqrt{2} & 1/\sqrt{2} & 0 \end{bmatrix}$	$\mathcal{E}_F \begin{bmatrix} 0 & 1/\sqrt{2} & 0 \\ 1/\sqrt{2} & 1/\sqrt{2} & 0 \\ 0 & 0 & -1/\sqrt{2} \end{bmatrix}$
$F(\mathrm{TO})_2$	$\mathcal{E}_F \begin{bmatrix} 0 & 1 & 0 \\ 1 & 0 & 0 \\ 0 & 0 & 0 \end{bmatrix}$	$\mathcal{E}_F \begin{bmatrix} 0 & 0 & -1 \\ 0 & 0 & 0 \\ -1 & 0 & 0 \end{bmatrix}$

volving phonons from the entire Brillouin zone are limited by the selection rule that the sum of the wave vectors of the participating phonons must be zero. Thus the first-order Raman effect results in a line spectrum, whereas the higher-order processes yield a quasicontinuous spectrum with features characterizing the critical points in the joint density of states. Typically the second-order spectra are weaker than the first order, have a background of continuum, and the sharp features are nonetheless broader than the lines observed in the first order. Thus, in the present study, the line spectra observed in $Bi_{12}GeO_{20}$ and $Bi_{12}SiO_{20}$ excited with the He-Ne laser will be interpreted as first-order spectra.

The number of zone-center phonons and their symmetry classification according to the irreducible representations of the crystal symmetry can be deduced by a group-theoretical analysis. The crystal structure of $Bi_{12}GeO_{20}$ and $Bi_{12}SiO_{20}$ shows[3] that the primitive unit cell contains one formula unit of $Bi_{12}MO_{20}$, where $M \equiv$ Ge or Si. The site symmetries are $M(T)$, $12\mathrm{Bi}(C_1)$, $12\mathrm{O_I}(C_1)$, $4\mathrm{O_{II}}(C_3)$, $4\mathrm{O_{III}}(C_3)$; here $\mathrm{O_I}$, $\mathrm{O_{II}}$, and $\mathrm{O_{III}}$ are the three nonequivalent sets of oxygen atoms. Using the method of coupling given by Couture and Mathieu[24] or the technique used by Bhagavantam and Venkatarayudu,[25] it can be shown that there are $8A$ (totally symmetric), $8E$ (doubly degenerate), and $24F$ (triply degenerate) zone-center optical phonons. Phonons of all the three symmetries are Raman active in the first order, and only those belonging to F symmetry are infrared active in the first order. Long-range polarization fields are expected to split the F modes into longitudinal-optic (LO) and transverse-optic (TO) phonons, with the former at a higher frequency.[23] The polarizability tensors for all the three symmetries are given in Table I for the two crystallographic orientations studied in this investigation. The polarization associated with F tensors, for the cubic orientation, is given in parentheses. The polarizability tensors for LO-TO-split F modes have been obtained explicitly by Poulet,[26] and these are given in Table II for the two orientations.

Chandrasekharan[27] has shown that optical activity in crystals, rather than being a hindrance, can be exploited to make symmetry assignments for Raman lines. In Fig. 1, $X0$ is the direction of the incident light, $0Y$ the direction of the scattered light, and φ the angle made by the electric vector of the incident light with the scattering plane. Then, the total scattered intensity I_{tot} as well as the part polarized parallel (I_H) and the part polarized perpendicular (I_V) to the scattering plane can be calculated as a function of φ for all three symmetries. Table III gives the intensity variations expected for each symmetry, for the two crystalline orientations. Thus, while using a fairly small length of sample—say, ~1 mm—along the incident direction, the variation in φ may be produced externally and the accompanying intensity variations observed, sitting on the peak of a given Raman line. In contrast to

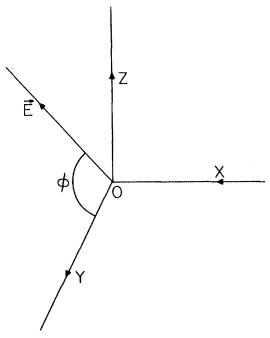

FIG. 1. Right-angle Raman scattering geometry, where the electric vector of the incident radiation makes an angle φ with the scattering plane.

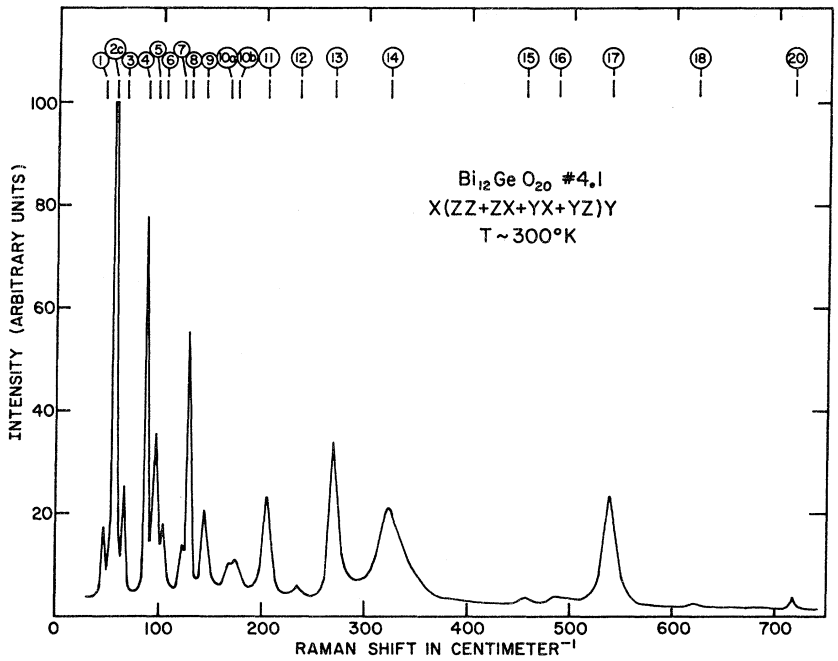

FIG. 2. Raman spectrum of $Bi_{12}GeO_{20}$ at room temperature. The spectrum was excited with ~50 mW of circularly polarized 6328-Å radiation from a He-Ne laser. X, Y, and Z are along the cubic directions. No analyzer was used in the path of the scattered radiation.

polarization measurements, optical activity along the scattered direction is no hindrance here. Also, the measurement of the phase of the oscillation pattern provides an absolute quantitative criterion as opposed to the qualitative measurement of depolarization ratios. Results obtained in $Bi_{12}GeO_{20}$ using this technique are discussed in the next section.

IV. EXPERIMENTAL RESULTS AND DISCUSSION

Figures 2–4 show the Raman spectra of $Bi_{12}GeO_{20}$ at 300, 77, and 15 °K, respectively, obtained for a crystal with {100} faces and with circularly polarized exciting radiation which was multipassed through the sample. Figures 5–7 show the spectra of $Bi_{12}SiO_{20}$ obtained under similar conditions. Use

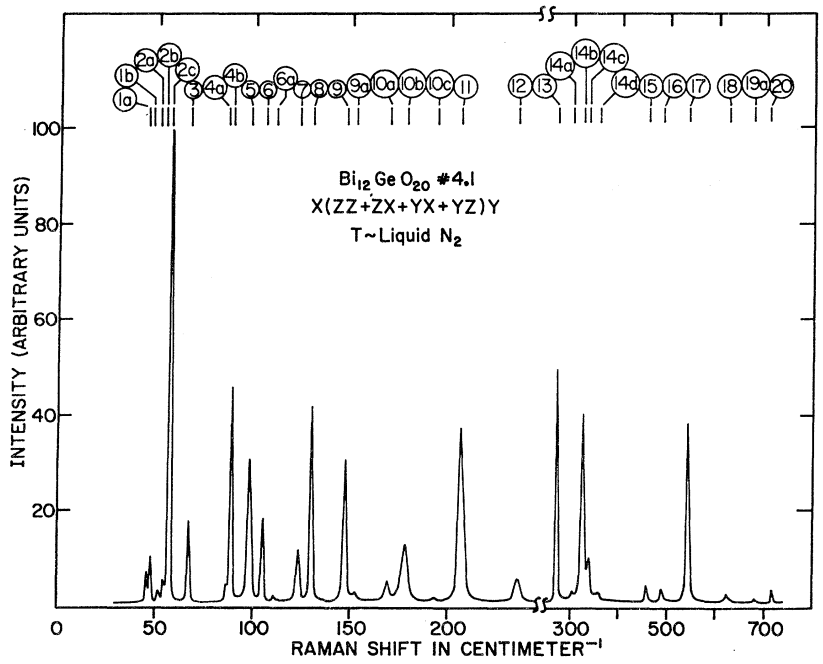

FIG. 3. Raman spectrum of $Bi_{12}GeO_{20}$ at 77 °K. Experimental conditions same as those for Fig. 2.

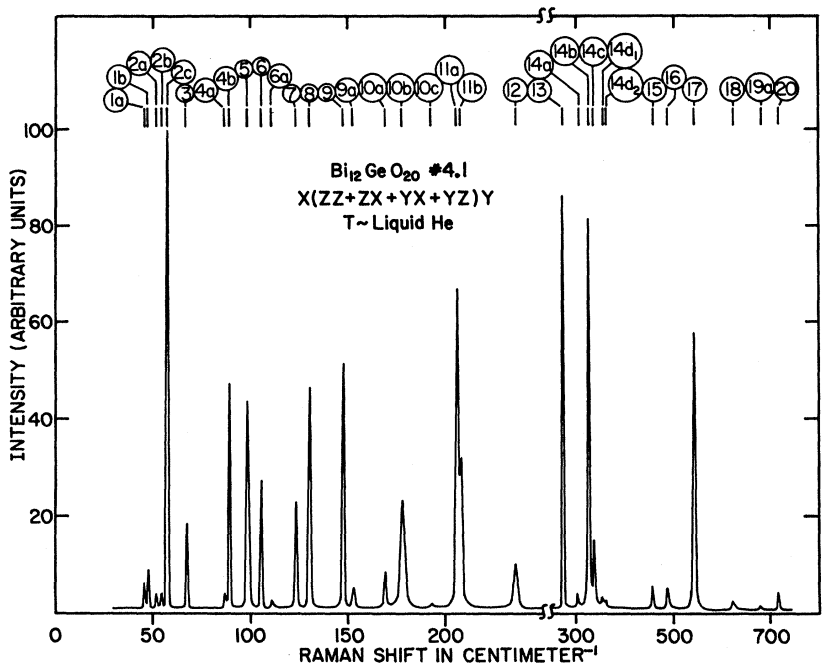

FIG. 4. Raman spectrum of $Bi_{12}GeO_{20}$ at 15 °K. Experimental conditions same as those for Fig. 2.

of circularly polarized incident light ensures that the state of polarization is the same throughout the length of the crystal. Thus the intensity observed for a given line for the various temperatures is not affected by the changes in optical activity, if any, with temperature; no restriction on the length of the sample along the incident light is necessary in contrast to polarization measurements with linearly polarized incident light. Under these conditions it was possible to record the entire Raman spectrum, including the weaker lines, under the best signal-to-noise ratio. Since complete Raman spectra were sought in these measurements, no analyzer was used in the scattered radiation. Thus the polarization characteristics of spectra in Figs. 2–8 may be described as $X(ZZ+YZ+YX+ZX)Y$, following the notation of Tell *et al.*[28] From Table I it is clear that in this configuration phonons belonging to all

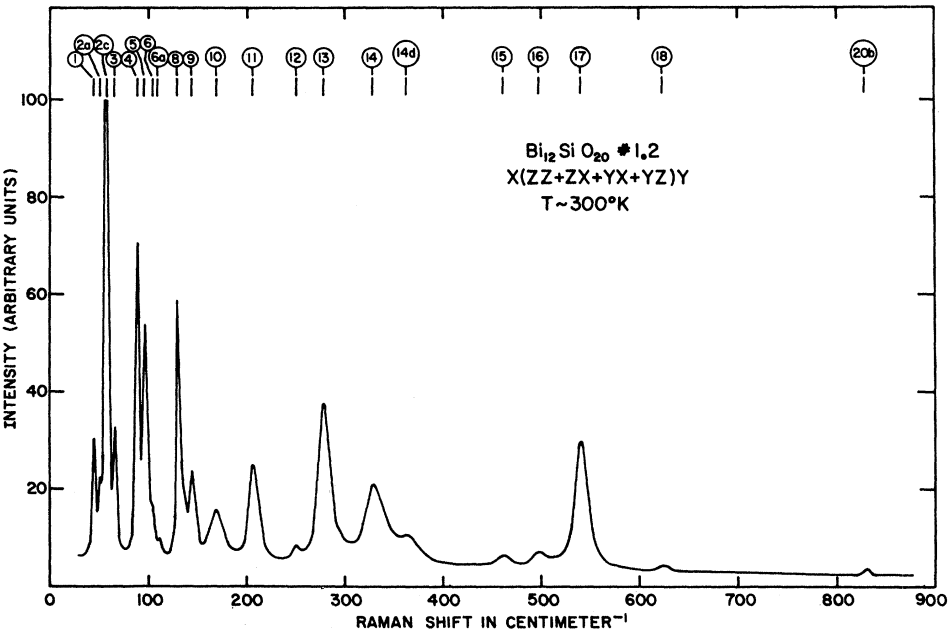

FIG. 5. Raman spectrum of $Bi_{12}SiO_{20}$ at room temperature. Experimental conditions same as those for Fig. 2.

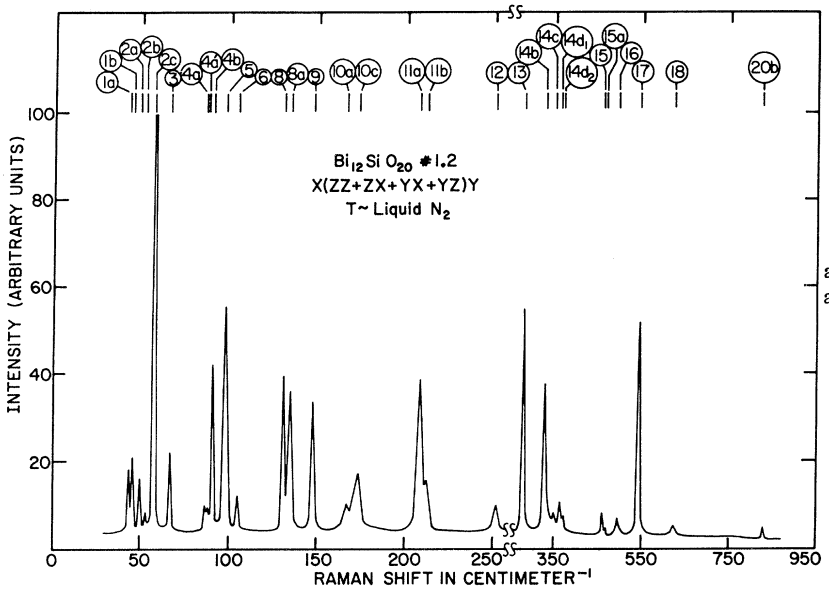

FIG. 6. Raman spectrum of $Bi_{12}SiO_{20}$ at 77 °K. Experimental conditions same as those for Fig. 2.

the three symmetries will be observed. It should be pointed out that the spectra shown in Figs. 2–7 have not been corrected for polarization and wavelength response of the spectrometer. Any temperature-dependent changes in the optical activity of the crystal can alter the extent of rotation suffered by the polarization of the scattered radiation through the crystal. Hence the observed spectra must be corrected for such polarization changes in the scattered radiation. Figures 2–7 have not been corrected for such possible effects. The results seem to indicate that such corrections are not important.

The rather sharp and strong line at 57.5 cm^{-1} in both $Bi_{12}GeO_{20}$ and $Bi_{12}SiO_{20}$ appears truncated in Figs. 2–7 as a result of the scale chosen. The variation of its intensity at the three temperatures is shown separately in Figs. 8 and 9 for $Bi_{12}GeO_{20}$ and $Bi_{12}SiO_{20}$ respectively. The intensity of a one-phonon Stokes process is proportional[23] to n_0+1, where the Bose-Einstein factor

$$n_0 = 1/(e^{(\hbar\omega/kT)} - 1) \quad (1)$$

and $\hbar\omega$ is the energy of the phonon under consideration. Thus a low-frequency line is expected to show a marked decrease in intensity on lowering the temperature of the crystal. Relative intensities measured for the intense, low-frequency line at 57.5 cm^{-1} in both $Bi_{12}GeO_{20}$ and $Bi_{12}SiO_{20}$ are consistent

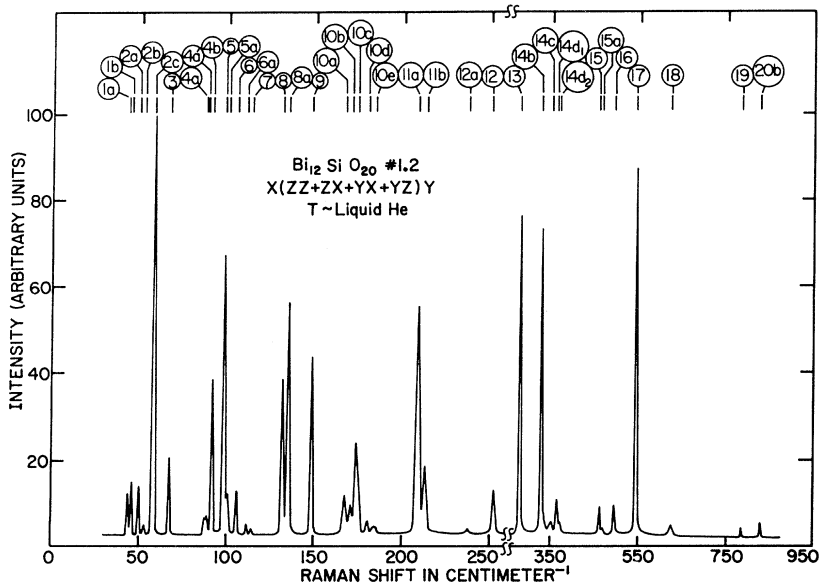

FIG. 7. Raman spectrum of $Bi_{12}SiO_{20}$ at 15 °K. Experimental conditions same as those for Fig. 2.

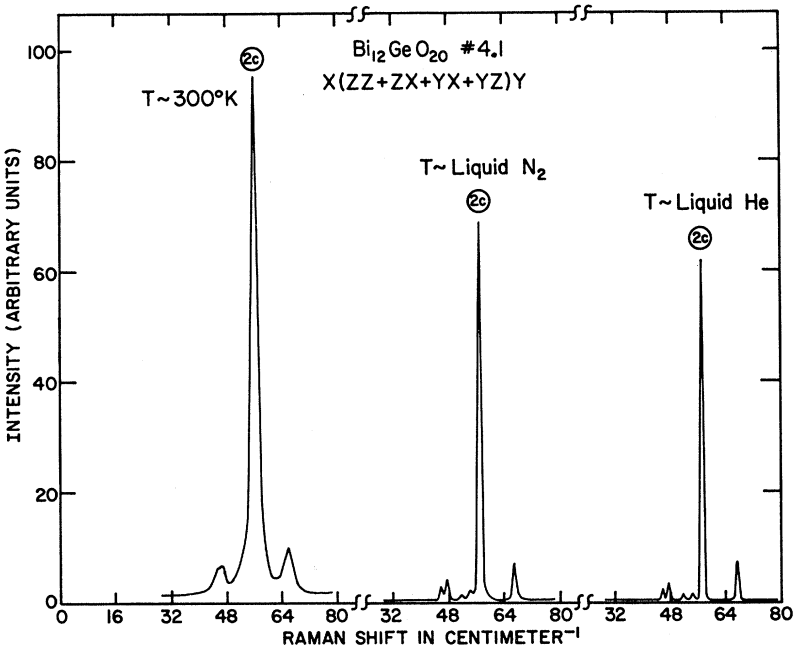

FIG. 8. Variation of intensity with temperature for the 57.5-cm^{-1} (2*c*) line of $Bi_{12}GeO_{20}$. Experimental conditions same as those for Fig. 2.

with this prediction. On the other hand, the integrated intensity of the lines at 546.2 cm^{-1} in $Bi_{12}SiO_{20}$ and at 542.6 cm^{-1} in $Bi_{12}GeO_{20}$ shows little variation as a function of temperature, as is to be expected for high-frequency lines.

The spectra of $Bi_{12}GeO_{20}$ and $Bi_{12}SiO_{20}$ have many common features in their temperature variation. On going from room to liquid-nitrogen temperature, most of the lines show some shift to higher frequencies. In addition, a marked sharpening is noticed, resulting in many of the broad room-temperature lines being resolved into a complex of sharp lines. For example, in $Bi_{12}GeO_{20}$, lines labeled 14*a*, 14*b*, 14*c*, and 14*d* were observed at room temperature as a very broad line centered at 324.1 cm^{-1}. On lowering the temperature to 15 °K using liquid helium as coolant, most lines sharpen still further, but no significant frequency shifts are seen. In

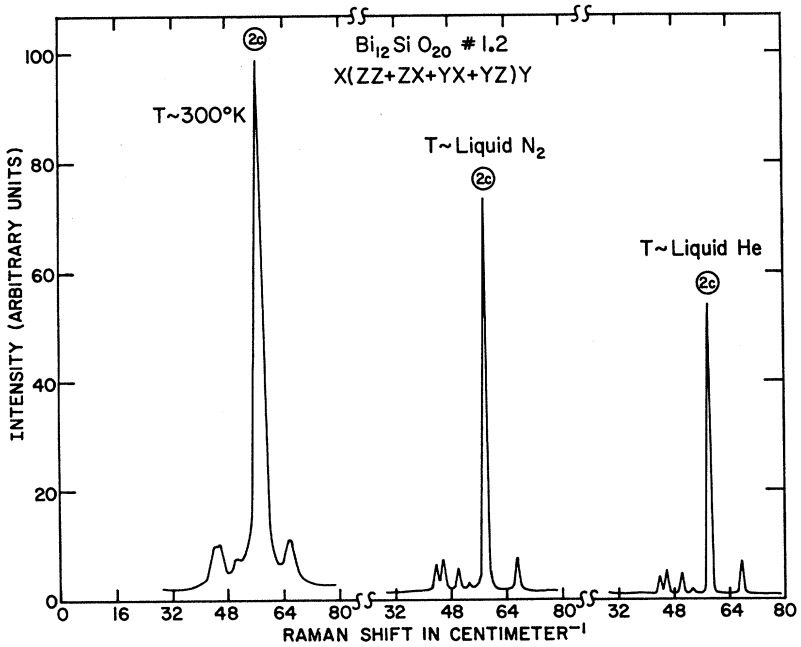

FIG. 9. Variation of intensity with temperature for the 58.0-cm^{-1} (2*c*) line of $Bi_{12}SiO_{20}$. Experimental conditions same as those for Fig. 2.

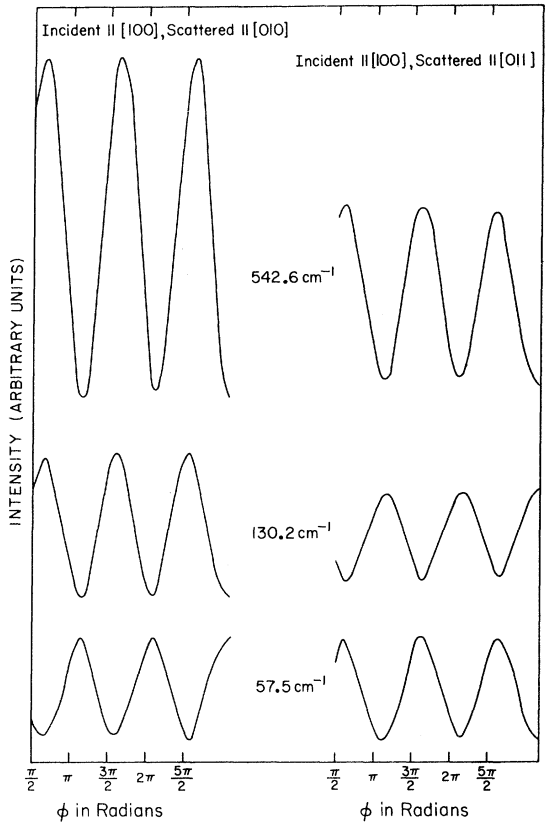

FIG. 10. Oscillations of intensity of the Raman lines 17 (542.6 cm^{-1}), 8 (130.2 cm^{-1}), and 2c (57.5 cm^{-1}) of $Bi_{12}GeO_{20}$ as a function of φ, the angle between the electric vector of the incident radiation and the plane of scattering (see also Fig. 1).

$Bi_{12}GeO_{20}$ the line at 207 cm^{-1} is seen to split into a doublet at 15 °K. Similarly, in $Bi_{12}SiO_{20}$, the features at 88.2, 100.7, 167.5, and 171.0 cm^{-1} observed at liquid-nitrogen temperature are resolved clearly at 15 °K.

We will now discuss the oscillations in the total scattered intensity of a given Raman line which occur when the plane of polarization of the exciting radiation is externally rotated. Figure 10 shows the results for three of the prominent lines of $Bi_{12}GeO_{20}$ for two crystallographic orientations. The results are to be compared with the predictions of Table III in order to deduce the symmetries of the lines. The oscillations are recorded with the initial polarization of the incident light at $\frac{1}{2}\pi$ with respect to the scattering plane. The period of the oscillations of all the lines is π, as is to be expected on elementary considerations. The positions of maxima and minima remain unaltered for the two scattering directions used in the case of the 542.6-cm^{-1} line. This is characteristic of a line with A symmetry. The oscillation pattern of the 130.2-cm^{-1} line is in phase with that of the A line for the [010] scattering direction, whereas it changes by $\frac{1}{2}\pi$ when the scattered light is observed along [011]. This behavior is characteristic of an E line. The 57.5-cm^{-1} line, on the other hand, exhibits oscillations out of phase by $\frac{1}{2}\pi$ with those of the A line for the [010] direction of scattering but in phase for the [011] direction of scattering. On this basis it is assigned F symmetry. Table IV summarizes symmetry assignments for the prominent lines of $Bi_{12}GeO_{20}$ deduced on the basis of this technique. These assignments are confirmed by polarization spectra as well, as we shall see further on.

From Table III, it should be noted that in the cubic-orientation A- and E-symmetry lines are expected to reach zero intensity at $\varphi = m\pi$, where m is an integer. Similarly, in the second orientation considered, A lines are expected to reach zero intensity at $\varphi = m\pi$. However, experimentally such perfect extinction of intensity was not observed; this can be attributed to the effects of finite collection angle of scattered radiation, slight crystal misorientation, and the finite optical activity within the sample length used along the incident direction. Also, the slight shift seen in Fig. 10, for the maxima and minima from $m\pi$ and $(2m+1)\frac{1}{2}\pi$, is due to the latter effect.

The intensity oscillations expected for an LO-TO-split F line, for each individual component, are also listed in Table III. It is seen that the angles

TABLE III. Variation in scattered intensity as a function of φ, the angle made by the electric vector of the incident radiation with the scattering plane.

	Incident ∥ [100], scattered ∥[010]			Incident ∥ [100], scattered ∥ [011]		
Symmetry	I_H	I_V	I_{tot}	I_H	I_V	I_{tot}
A	0	$a^2 \sin^2\varphi$	$a^2 \sin^2\varphi$	0	$a^2 \sin^2\varphi$	$a^2 \sin^2\varphi$
E	0	$4\mathcal{E}_E{}^2 \sin^2\varphi$	$4\mathcal{E}_E{}^2 \sin^2\varphi$	0	$\mathcal{E}_E{}^2(1+2\cos^2\varphi)$	$\mathcal{E}_E{}^2(1+2\cos^2\varphi)$
F(TO+LO)	$\mathcal{E}_F{}^2$	$\mathcal{E}_F{}^2 \cos^2\varphi$	$\mathcal{E}_F{}^2(1+\cos^2\varphi)$	$\mathcal{E}_F{}^2$	$\mathcal{E}_F{}^2 \sin^2\varphi$	$\mathcal{E}_F{}^2(1+\sin^2\varphi)$
F(TO)	$\frac{1}{2}\mathcal{E}_F{}^2(1+\cos^2\varphi)$	$\frac{1}{2}\mathcal{E}_F{}^2 \cos^2\varphi$	$\mathcal{E}_F{}^2(\frac{1}{2}+\cos^2\varphi)$	$\frac{1}{2}\mathcal{E}_F{}^2(1+\sin^2\varphi)$	$\frac{1}{2}\mathcal{E}_F{}^2 \sin^2\varphi$	$\mathcal{E}_F{}^2(\frac{1}{2}+\sin^2\varphi)$
F(LO)	$\frac{1}{2}\mathcal{E}_F{}^2 \sin^2\varphi$	$\frac{1}{2}\mathcal{E}_F{}^2 \cos^2\varphi$	$\frac{1}{2}\mathcal{E}_F{}^2$	$\frac{1}{2}\mathcal{E}_F{}^2 \cos^2\varphi$	$\frac{1}{2}\mathcal{E}_F{}^2 \sin^2\varphi$	$\frac{1}{2}\mathcal{E}_F{}^2$

TABLE IV. Symmetry assignments for prominent lines of $Bi_{12}GeO_{20}$ on the basis of the observed intensity oscillations as a function of ϕ.

A	E	F
89.4 (4b)	67.7 (3)	57.5 (2c)
148.0 (9)	130.2 (8)	99.0 (5)
273.0 (13)	236.5 (12)	178.5 (10b)
326.0 (14b)	458.3 (15)	207.0 (11a+11b)
542.6 (17)	623.1 (18)	

of maximum and minimum intensity for a TO mode are identical to those for an F mode, in both orientations. However, the theoretical ratio of minimum intensity to maximum intensity in the oscillations is $I_{min}/I_{max}=\frac{1}{2}$ for an F mode, whereas for a TO mode the ratio is $I_{min}/I_{max}=\frac{1}{3}$; this is the case for both crystallographic orientations. Experimentally, it is difficult to measure the ratio I_{min}/I_{max} with precision as a result of finite collection angle, slight crystal misorientation, and finite optical activity within the sample length used. Thus, in this investigation, it has not been possible to use the ratio I_{min}/I_{max} to distinguish F(TO) from an unsplit F line. Hence, at this stage, the lines labeled F in Table IV may be considered to have either F(LO+TO) symmetry or F(TO) symmetry. However, the polarization measurements discussed further on show that these all possess F(LO+TO) symmetry.

When the incident light is along a cubic direction, it can be seen from Table III that for A, E, and F(LO+TO) symmetries, scattered radiation polarized along the normal to the scattering plane is the only component which exhibits oscillations on rotating the plane of polarization of the incident light externally. Hence in the two crystallographic orientations considered here, the polarization response of the spectrometer is unimportant for the three symmetries mentioned above, as the oscillating part of the scattered intensity is polarized along a specific direction with respect to the grating grooves. For lines of F(TO) symmetry it can be seen that the oscillating part of the scattered intensity has both vertical and horizontal polarizations, in the two crystallographic orientations considered here. However, in both polarizations the intensity variation is described by the *same* function, i.e., $\cos^2\varphi$ or $\sin^2\varphi$, as the case may be. Hence the polarization response of the spectrometer can only affect the amplitude of the observed oscillations but not their functional behavior. For F(LO) symmetry, on the other hand, no variation in total scattered intensity as a function of φ is expected for both orientations, as seen from Table III. Any unequal response of the spectrometer for light polarized parallel to the grating grooves as compared to that polarized perpendicular to the grooves will cause residual intensity oscillations whose form is determined by the polarization favored by the grating. Thus it may be noted that an experimental check of the constancy of total intensity for F(LO) must include appropriate corrections for the polarization response of the spectrometer. In the wavelength region of these measurements, the spectrometer has a higher response for I_H compared to I_V. Hence the residual oscillations in the total intensity of F(LO) lines are determined by I_H for both orientations. Such oscillations will be in phase with the variations in total intensity for E lines, as can be seen from Table III. Nonetheless, such an ambiguity between F(LO) and E lines can be eliminated by observing I_H and I_V separately, using an analyzer in the scattered radiation. In this study, for lines assigned the E symmetry in Table IV, I_H and I_V were not separately observed, as independent confirmation for these assignments was obtained from polarization studies.

The symmetry classification of the observed lines in the spectra of $Bi_{12}GeO_{20}$ and $Bi_{12}SiO_{20}$ using conventional polarization measurements will now be discussed. These have been carried out by choosing appropriately the polarizations of the incident and the scattered radiation as well as the crystallographic orientation for a given scattering geometry. By this method, phonons of a desired symmetry can be selectively observed. From Table I it is seen that in the cubic orientation the polarizability tensors of A and E symmetry are diagonal, whereas the tensors of F symmetry contain only off-diagonal elements. Thus the $X(ZZ)Y$ spectrum shows scattering from A and E modes. For the polar F modes, one must consider the polarization and propagation directions of the phonon simultaneously in order to distinguish their TO or LO character. Thus, in the cubic orientation, it can be seen that for the $X(YZ)Y$ scattering geometry, the phonon polarization associated with the tensor component α_{YZ} lies along the X direction. As the propagation direction of the phonon, which is in the XY plane, makes an angle of 45° with the X direction, it is clear that the phonon polarization can be resolved into two components, one parallel and the other perpendicular to the propagation direction. Hence the $X(YZ)Y$ spectrum shows scattering from both F(LO) and F(TO) modes. In contrast, in the back-scattering geometry $X(ZY)\bar{X}$, the propagation and polarization directions of the phonon coincide, both of them lying along the X direction. Thus the $X(ZY)\bar{X}$ spectrum arises from scattering from F(LO) phonons alone. From similar considerations, it can be seen that the $X(ZX)Y$ spectrum shows scattering from both F(TO) and F(LO) modes, while $X(YX)Y$ spectrum shows scattering from F(TO) modes only.

On transforming the polarizability tensors by a 45° rotation about the [100] direction, it is found

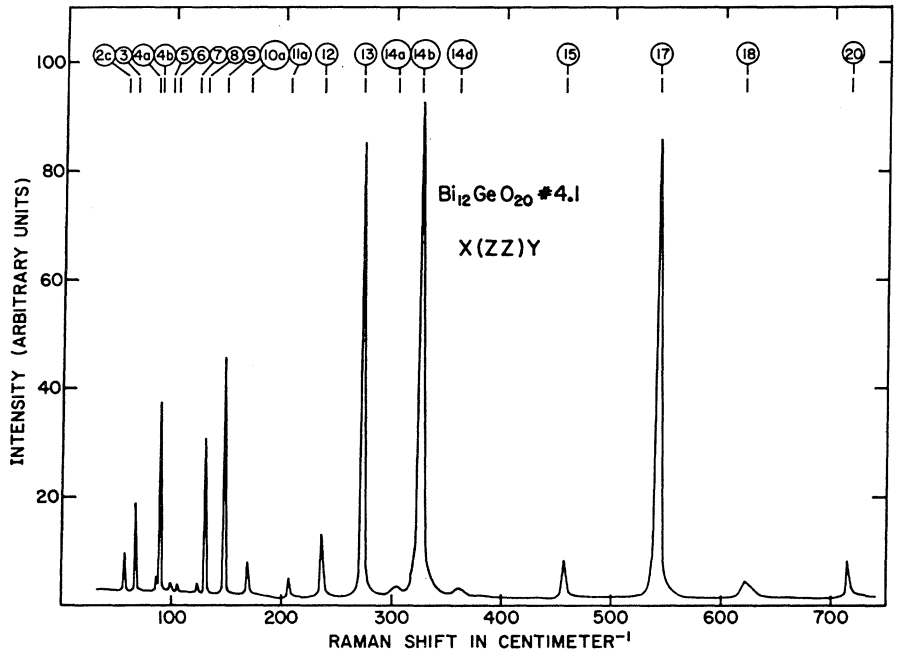

FIG. 11. $X(ZZ)Y$ scattering in $Bi_{12}GeO_{20}$; $T \sim 15\,^{\circ}K$. X, Y, and Z are along the cubic directions.

that only the E tensors acquire off-diagonal components $\alpha_{Y'Z'}$; here X, Y', and Z' are [100], [011], and [0$\bar{1}$1], respectively. Thus the $X(Y'Z')Y'$ spectrum arises from scattering from phonons of E symmetry, and modes of A and F symmetry will not be seen in this polarization. Hence phonons of E symmetry can be separated from those of A symmetry by a direct comparison with $X(ZZ)Y$ spectrum. From Table II it should be noted that an F(TO) spectrum can also be excited in the $X(Z'X')Y'$ configuration.

Since the most detailed spectra of $Bi_{12}GeO_{20}$ and $Bi_{12}SiO_{20}$ with well-resolved lines were observed at $T \sim 15\,^{\circ}K$, all the polarization measurements reported here were carried out at this temperature. In addition, the polarization spectra presented are corrected for the polarization and wavelength responses of the spectrometer. It should be remarked

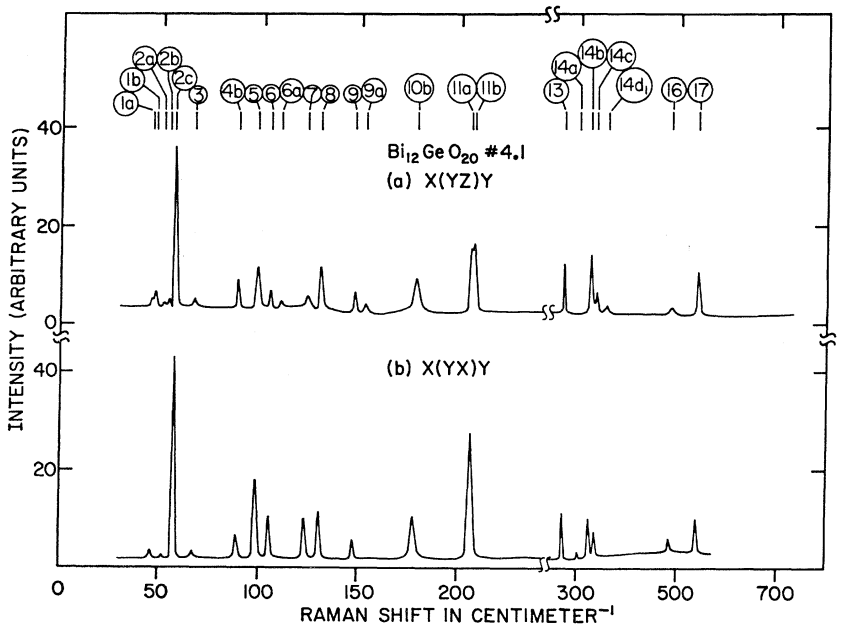

FIG. 12. Raman spectrum of $Bi_{12}GeO_{20}$; $T \sim 15\,^{\circ}K$; (a) $X(YZ)Y$, (b) $X(YX)Y$. X, Y, and Z are along the cubic directions.

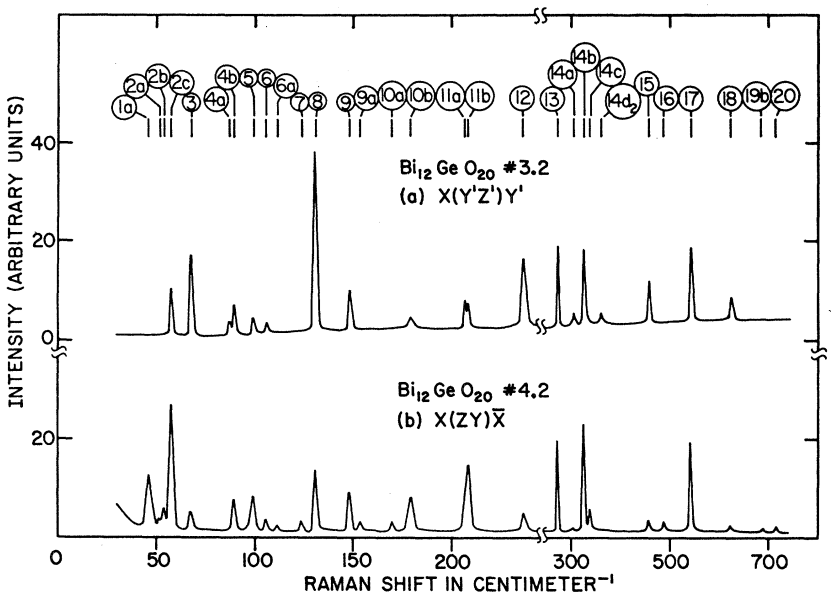

FIG. 13. Raman spectrum of $Bi_{12}GeO_{20}$; $T \sim 15\,^{\circ}K$; (a) $X(Y'Z')Y'$, (b) $X(ZY)\bar{X}$. X, Y, and Z are along the cubic directions and $X \parallel [100]$, $Y' \parallel [011]$, $Z' \parallel [0\bar{1}1]$.

that considerable depolarization effects were observed in polarization spectra, resulting in spillover of intensity from forbidden symmetries. This arises from the finite rotation of the plane of polarization suffered by the incident and scattered radiation in the crystal. In addition, the finite collection angle of scattered radiation and any slight crystalline misorientation can be contributory factors to the spillover of intensity. Despite these difficulties, it was possible to make unambiguous assignments for most of the lines by comparing the intensity of a given line for the various polarizations. It should be pointed out that in this manner it is possible to determine only the symmetry of a line, but not the magnitude of the tensor components associated with it.

Figures 11–13 show the various polarization spectra observed in $Bi_{12}GeO_{20}$, plotted on the same intensity scale. In Fig. 11, it is seen that lines at 130.2 cm^{-1} (8), 147.5 cm^{-1} (9), and 542.6 cm^{-1} (17) are all prominent. All three lines are considerably attenuated in the polarizations where only the F modes should appear, and thus the three lines have A or E symmetry. However, it is seen in Fig. 13 (a) that only the 130.2-cm^{-1} (8) line retains its intensity, and thus it must have E symmetry. The other two lines are much weaker in this polarization and are hence assigned A symmetry. A com-

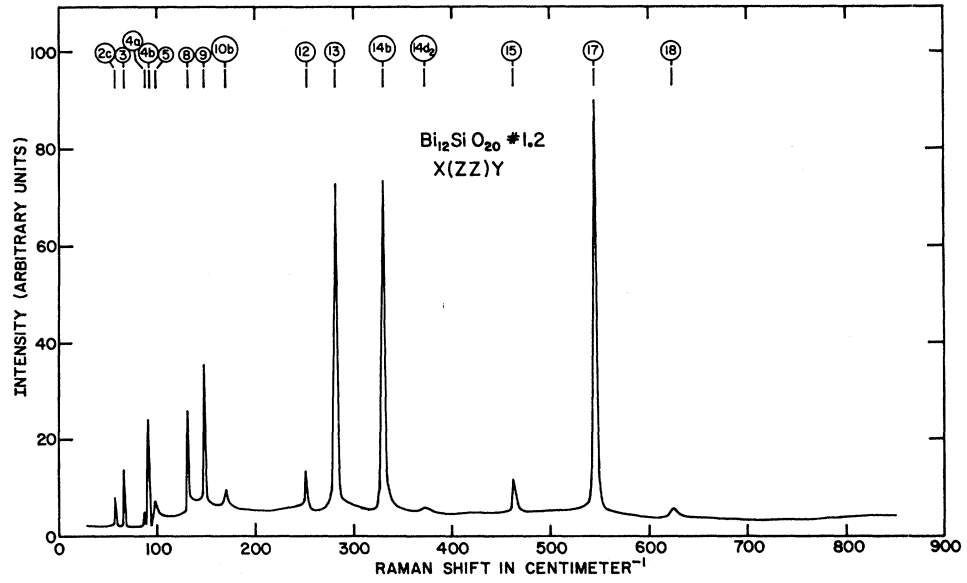

FIG. 14. $X(ZZ)Y$ scattering in $Bi_{12}SiO_{20}$; $T \simeq 15\,^{\circ}K$. X, Y, and Z are along the cubic directions.

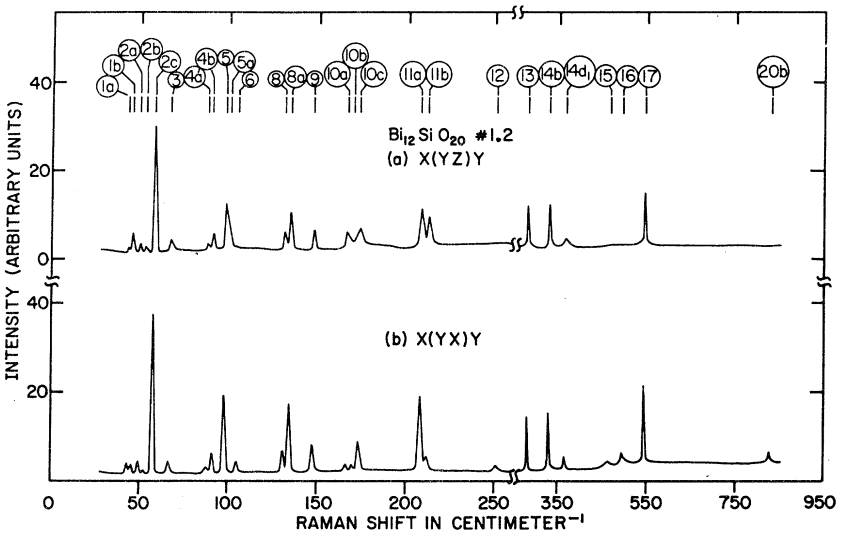

FIG. 15. Raman spectrum of $Bi_{12}SiO_{20}$; $T \sim 15\,^{\circ}K$; (a) $X(YZ)Y$, (b) $X(YX)Y$. X, Y, and Z are along the cubic directions.

parison of the intensity of the line at 57.5 cm^{-1} ($2c$) in the various polarizations clearly establishes its symmetry as $F(LO+TO)$. In a similar manner, the pair of lines at 206.5 cm^{-1} ($11a$) and 208.0 cm^{-1} ($11b$) are seen to belong to F symmetry. The absence of ($11b$) in $X(YX)Y$ shows it to be $F(LO)$. In the $X(ZY)\bar{X}$ polarization, the line at 208.0 cm^{-1} appears strong, while the line at 206.5 cm^{-1} is weaker in comparison. Thus line ($11a$) has $F(TO)$ symmetry and line ($11b$) has $F(LO)$ symmetry.

In Fig. 11, the line at 147.5 cm^{-1} (9) is more intense than the line at 130.2 cm^{-1} (8). If line (8) has pure E symmetry, the intensity spillover of line (8) must continue to be less than that for line (9), in the polarizations where F modes appear. This is not the case, however, and line (8) is more intense than the spillover for line (9) in all polarizations where F modes are observed. In addition, line (8) occurred in all these polarizations at 131.2 ± 0.5 cm^{-1}. This shows that a weaker line of $F(LO+TO)$ symmetry is nearly degenerate in energy with the line of E symmetry at 130.2 cm^{-1}, within experimental accuracy. As we shall see below, the presence of a line of $F(LO+TO)$ symmetry at 135.2 cm^{-1} ($8a$) very close to the E-symmetry line at 131.8 cm^{-1} (8), in $Bi_{12}SiO_{20}$, lends further support to this conclusion of near degeneracy of lines of E and F symmetry at 130.2 cm^{-1} in $Bi_{12}GeO_{20}$. These examples illustrate the basis on which symmetry assignemnts were determined for all the observed lines.

The various polarization spectra observed in $Bi_{12}SiO_{20}$, plotted on a common intensity scale, are shown in Figs. 14–16. In Fig. 14, the slight increase

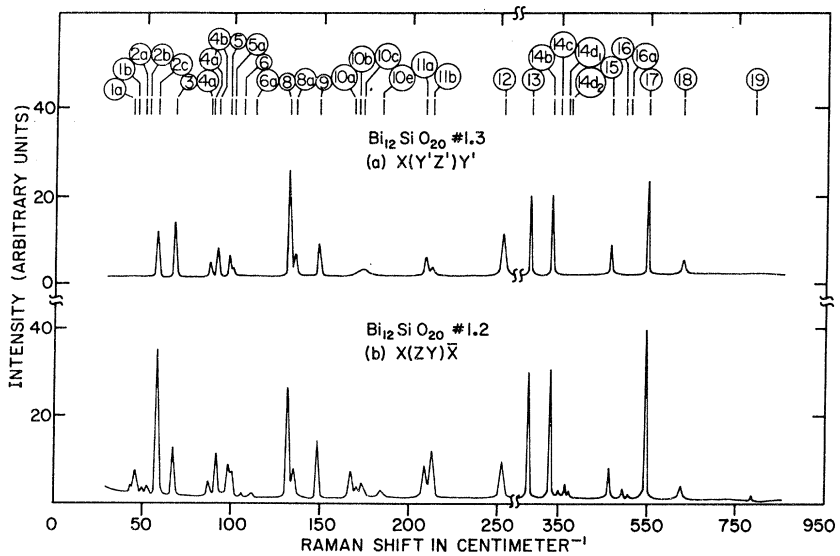

FIG. 16. Raman spectrum of $B_{12}SiO_{20}$; $T \sim 15\,^{\circ}K$; (a) $X(Y'Z')Y'$, (b) $X(ZY)\bar{X}$. X, Y, and Z are along the cubic directions and $X \parallel [100]$, $Y' \parallel [011]$, $Z' \parallel [0\bar{1}1]$.

TABLE V. Symmetry assignments for the Raman lines of $Bi_{12}GeO_{20}$. The line labels are indicated in parentheses.

A	E	F	
89.4 (4b)	67.7 (3)	46.4 (1a)	TO + LO
148.0 (9)	97.2 (4a)	48.1 (1b)	LO
170.0 (10a)	130.2 (8)	52.4 (2a)	TO + LO
273.0 (13)	236.5 (12)	54.6 (2b)	LO
326.0 (14b)	306.2 (14a)	57.5 (2c)	TO + LO
542.6 (17)	360.6 (14d_2)	99.0 (5)	TO + LO
715.1 (20)	458.3 (15)	105.8 (6)	TO + LO
	623.1 (18)	111.2 (6a)	LO
		124.0 (7)	TO + LO
		131.2 (8)	TO + LO
		153.0 (9a)	LO
		178.5 (10b)	TO + LO
		194.4 (10c)	LO
		207.0 (11a)	TO
		208.5 (11b)	LO
		305.0 (14a)	TO + LO
		338.0 (14c)	TO + LO
		357.5 (14d_1)	TO + LO
		488.3 (16)	TO + LO
		678.6 (19a)	TO + LO
		691.8 (19b)	LO

in background, observed in the region 100–200 cm^{-1}, is of instrumental origin. The lines have been labeled so as to emphasize as far as possible the striking similarities in line positions and symmetries as compared to those of $Bi_{12}GeO_{20}$, for most of the prominent lines. As an example, the foregoing comments on lines (2c), (9), (11a), (11b), and (17) apply in the case of $Bi_{12}SiO_{20}$ as well, and though the positions of these lines differ slightly, their symmetries are identical in both crystals. Tables V and VI list, for $Bi_{12}GeO_{20}$ and $Bi_{12}SiO_{20}$, respectively, the positions of the observed Raman lines at 15 °K and their assigned symmetries. The line labels appear in parentheses following the line positions. The assignments for the weaker lines were determined in both crystals by studying their polarization characteristics individually under appropriate slit width and gain conditions. In the case of extremely weak lines, the proposed assignments are tentative, as indicated by a question mark. A search at 15 °K up to a shift of 3000 cm^{-1} revealed no Raman lines in both crystals other than those reported here.

It is of interest to analyze the observed spectra of $Bi_{12}GeO_{20}$ and $Bi_{12}SiO_{20}$ from a dynamical viewpoint. The crystal structure of [2] $Bi_{12}SiO_{20}$ is identical to that of $Bi_{12}GeO_{20}$.[3] The lattice parameter for the cubic unit cell is 10.098 ± 0.004 Å for $Bi_{12}SiO_{20}$ and 10.1455 ± 0.0008 Å for $Bi_{12}GeO_{20}$. Thus the unit-cell parameter of $Bi_{12}SiO_{20}$ differs from that of $Bi_{12}GeO_{20}$ by only ~0.5%. Structurally, the only other difference is that the central atom in the unit cell is Ge in one case and Si in the other. In both cases, the central atom has four nearest-neighbor oxygen atoms, thus forming an MO_4 tetrahedron, where $M \equiv$ Ge or Si. In the approximation that the MO_4 group may be considered as a tightly bound molecular unit, the zone-center phonons of the crystal may be divided into those originating from the normal modes of the MO_4 unit and the rest being the modes where the entire MO_4 unit vibrates against the other atoms in the crystal. MO_4 as a free unit with T_d symmetry has $A_1 + E + 2F_2$ normal modes; translations and rotations of this unit belong to F_2 and F_1, respectively. On being incorporated in $Bi_{12}GeO_{20}$ or $Bi_{12}SiO_{20}$, the site symmetry of MO_4 becomes T, which is of a lower symmetry than T_d. However, this does not lead to lifting of the degeneracies in the normal modes of the MO_4 unit, since the correlation of the normal modes of the MO_4 unit in the crystal is given by $A + E + 4F$; two of the F modes arise from the translatory and rotatory motions acquiring nonzero frequencies when MO_4 becomes a part of the crystal. It should be pointed out that the F modes might undergo LO-TO splitting as a result of the long-range polarization fields in the crystal. A knowledge of the frequencies of the normal modes of the GeO_4 unit and the SiO_4 unit would be very useful for a direct comparison with the observed frequencies in $Bi_{12}GeO_{20}$

TABLE VI. Symmetry assignments for the Raman lines of $Bi_{12}SiO_{20}$. The line labels are indicated in parentheses.

A	E	F	
91.7 (4b)	68.0 (3)	44.4 (1a)	TO + LO
148.7 (9)	87.7 (4a)	46.1 (1b)	LO
170.7 (10b)	131.8 (8)	50.6 (2a)	TO + LO
282.1 (13)	252.0 (12)	53.5 (2b)	LO
330.8 (14b)	372.6 (14d_2)	58.0 (2c)	TO + LO
546.2 (17)	463.6 (15)	89.2 (4a')	TO + LO
785.0 (19)	626.3 (18)	98.8 (5)	TO
817.5 (?) (20a)		100.7 (5a)	LO
		105.7 (6)	TO + LO
		112.4 (6a)	LO
		114.4 (7)	F or TO
		117.8 (7a)	F (?)
		135.5 (8a)	TO + LO
		167.0 (10a)	LO
		174.0 (10c)	TO
		180.7 (10d)	LO (?)
		185.0 (10e)	LO
		195.6 (10f)	F (?)
		209.0 (11a)	TO
		213.0 (11b)	LO
		238.0 (12a)	F or TO
		352.3 (14c)	TO + LO
		367.2 (14d_1)	TO + LO
		469.3 (15a)	F (?)
		495.6 (16)	TO + LO
		509.1 (16a)	TO + LO
		827.4 (20b)	TO
		841.0 (20c)	LO

TABLE VII. Calculated normal-mode frequencies of the MO_4 unit, where M = Si or Ge, and the corresponding assigned frequencies in $Bi_{12}SiO_{20}$ and $Bi_{12}GeO_{20}$. The site symmetry of free MO_4 is T_d, while in the crystal it becomes T.

Symmetry T_d	Symmetry T	SiO_4 (calculated) (cm^{-1})	$Bi_{12}SiO_{20}$ (observed) (cm^{-1})	GeO_4 (calculated) (cm^{-1})	$Bi_{12}GeO_{20}$ (observed) (cm^{-1})
A_1	A	749	785.0 (19)	749	715.1 (20)
E	E	461	463.6 (15)	461	458.3 (15)
F_1	F	374	367.2 ($14d_1$)	374	357.5 ($14d_1$)
F_2	F	224	238.0 (12a)	173	178.5 (10b)
F_2	F	528	495.6 (16)	481	488.3 (16)
F_2	F	911	...	804	...

and $Bi_{12}SiO_{20}$, respectively. However, conclusive experimental results are not available concerning the frequencies of the GeO_4 or SiO_4 unit. The recent study of Dawson *et al.*[29] on the vibrational spectrum of zircon ($ZrSiO_4$) treats the SiO_4 ion as a tightly bound molecular unit. From a study of the polarized infrared and Raman spectra of zircon, they found that the crystal field splittings of the SiO_4 vibrational levels are rather large. Without a detailed knowledge of the perturbations due to the crystal field in zircon, one cannot estimate the vibrational frequencies of the free SiO_4 ion in such a case where large splittings exist. Thus, the alternative is to adopt a model in order to estimate the vibrational frequencies of the MO_4 unit. This has been carried out by Wadia and Balloomal[30] for a SiO_4 unit. Using only the direct force constants and neglecting the interaction constants, they have obtained expressions for the normal-mode frequencies of the SiO_4 unit. In this model, the vibrational frequencies of A_1, E, F_1, modes of the MO_4 unit are independent of the mass of the central atom, and only the three F_2 modes depend on silicon or germanium atomic mass. Using the polarization characteristics and frequencies of the infrared and Raman bands observed in fused silica as a guide, they have chosen a set of values for the direct force constants. The frequencies calculated in this manner are in fair agreement with the observed bands in fused silica. Considering the fact that the vibrational spectra of fused silica are rather broad and quasicontinuous, the experimental line positions are not as accurate as those reported in this study. Nevertheless, the frequencies calculated by them for the A_1, E, and F_1 modes can serve as a useful guide in locating modes of corresponding symmetry in $Bi_{12}GeO_{20}$ and $Bi_{12}SiO_{20}$ in the appropriate frequency regions. Empirically, the following set of values in units of 10^5 dyn/cm chosen for the direct force constants was found to give reasonable agreement between calculated and observed frequencies: $C_r = 3.5$, $C_d = 1.8$, $C_\alpha = 0.23$, and $C_\beta = 0.22$. Table VII shows the calculated frequencies for GeO_4 and SiO_4 units along with the lines assigned as the corresponding observed frequencies in $Bi_{12}GeO_{20}$ and $Bi_{12}SiO_{20}$, respectively. In view of the empirical nature of the calculations giving the freuqencies of the MO_4 unit, the assigned frequencies in Table VII must be regarded as tentative. An inspection of Tables V and VI shows that the foregoing approach can account for certain features of the spectra of $Bi_{12}GeO_{20}$ and $Bi_{12}SiO_{20}$.

In view of the large number of phonons of F symmetry in these crystals, it should be of interest to study the infrared as well as polariton Raman spectra of $Bi_{12}GeO_{20}$ and $Bi_{12}SiO_{20}$. Piezospectroscopic effects[31] should also be observable in these crystals in view of the rather sharp and prominent lines seen at low temperatures. The second-order Raman spectra of these crystals, though expected to be weak, will overlap with the region of first-order spectra, and thus it might be interesting to investigate possible interference effects between the two.[32]

ACKNOWLEDGMENTS

The authors are grateful to Miss Louise Roth for growing some of the crystals used in this study. Thanks are due to Professor H. J. Yearian for orienting crystals and to Dr. A. Jayaraman and Professor P. Fisher for discussions.

*Work supported by the National Science Foundation and the Advanced Research Projects Agency.

[1]A. A. Ballman, J. Crystal Growth 1, 37 (1967).

[2]A. I. Safonov, S. A. Baryshev, T. I. Nikiforova, G. N. Antonov, and S. A. Fedulov, Kristallografiya 13, 914 (1968) [Sov. Phys. Cryst. 13, 797 (1969)].

[3]S. C. Abrahams, P. B. Jamieson, and J. L. Bernstein, J. Chem. Phys. 47, 4034 (1967).

[4]P. V. Lenzo, E. G. Spencer, and A. A. Ballman, Appl. Opt. 5, 1688 (1966).

[5]A. Feldman, W. S. Brower, Jr., and D. Horowitz, Appl. Phys. Letters 16, 201 (1970).

[6]S. Chandrasekhar, Proc. Roy. Soc. (London) A259, 531 (1961).

[7]M. Onoe, A. W. Warner, and A. A. Ballman, IEEE Trans. Sonics Ultrason. SU-14, 165 (1967).

[8]W. G. Cady, *Piezoelectricity* (Dover, New York, 1964), Vol. 1, p. 229.
[9]R. Nitsche, J. Appl. Phys. 36, 2358 (1965).
[10]Brief reports were given in S. Venugopalan and A. K. Ramdas, Phys. Letters 34A, 9 (1971); Bull. Am. Phys. Soc. 16, 334 (1971).
[11]Isomet Corp., 103 Bauer Drive, Oakland, N.J. 07436.
[12]The polishing accessories used are manufactured by Buehler Ltd., 2120 Greenwood St., Evanston, Ill. 60204.
[13]Spectra Physics, 1250 West Middlefield Road, Mountain View, Calif. 94040.
[14]Coherent Radiation Laboratories, 932 East Meadow Drive, Palo Alto, Calif. 94303.
[15]Jarrell-Ash Division, 590 Lincoln Street, Waltham, Mass. 02154.
[16]ITT Industrial Laboratories, Electron Tube Division, 3700 East Pontiac Street, Fort Wayne, Ind. 46803.
[17]S. A. Solin, Ph.D. thesis (Purdue University, 1970) (unpublished).
[18]P. Fisher, W. H. Haak, E. J. Johnson, and A. K. Ramdas, in *Proceedings of the Eighth Symposium on the Art of Glassblowing* (The American Scientific Glassblowers Society, Wilmington, Del., 1963), p. 136.
[19]Gaertner Scientific Corporation, 1201 Wrightwood Avenue, Chicago, Ill. 60614.
[20]J. F. Scott and S. P. S. Porto, Phys. Rev. 161, 903 (1967).
[21]S. A. Solin and A. K. Ramdas, Phys. Rev. 174, 1069 (1968).
[22]C. M. Hartwig, D. L. Rousseau, and S. P. S. Porto, Phys. Rev. 188, 1328 (1969).
[23]R. Loudon, Advan. Phys. 13, 423 (1964).
[24]L. Couture and J. P. Mathieu, J. Phys. Radium 10, 145 (1949). Note that the doubly degenerate mode is separably degenerate for the crystal symmetry $T(23)$.
[25]S. Bhagavantam and T. Venkatarayudu, Proc. Indian Acad. Sci. 9, 224 (1939).
[26]H. Poulet, Ann. Phys. (Paris) 10, 908 (1955).
[27]V. Chandrasekharan, Z. Physik 154, 43 (1959).
[28]B. Tell, T. C. Damen, and S. P. S. Porto, Phys. Rev. 144, 771 (1966).
[29]P. Dawson, M. M. Hargreave, and G. R. Wilkinson, J. Phys. C 4, 240 (1971).
[30]W. Wadia and L. S. Balloomal, Phys. Chem. Glasses 9, 115 (1968).
[31]V. J. Tekippe and A. K. Ramdas, Phys. Letters 35A, 143 (1971).
[32]See, for example, D. L. Rousseau and S. P. S. Porto, Phys. Rev. Letters 20, 1354 (1971).

PHYSICAL REVIEW B VOLUME 5, NUMBER 10 15 MAY 1972

Calculation of the Optical Constants for the Potassium Halides from Korringa-Kohn-Rostoker Energy Bands

H. Overhof*
IBM Research Laboratory, San Jose, California 95114
(Received 20 December 1971)

KKR energy bands are used to calculate joint densities of states for KCl, KBr, and KI between conduction states and valence and core states by means of a simple interpolation scheme. The results are discussed and compared with experimental spectra in the vacuum ultraviolet and soft-x-ray regions. An overall agreement between theory and experiment is found which suggests that strong exciton effects are present in excitations from p-like valence bands, but not from d bands.

I. INTRODUCTION

In the last five years low-temperature spectra of the potassium halides covering the fundamental absorption,[1–3] excitation from the potassium p levels[4–6] and from deeper core levels[7–10] have been published by several authors. Nevertheless, our knowledge of the energy bands which give rise to these spectra is very incomplete due to the fact that the various band models calculated by means of the orthogonalized-plane-wave (OPW),[11–13] augmented-plane-wave (APW),[14,15] pseudopotential,[16] and KKR[17,18] methods are very dissimilar in the shape and position of the higher conduction bands. Some features, however, are common in the band models and are supported by the experiments: (i) The valence bands are very flat with spin-orbit splittings of about 0.1, 0.5, and 1.1 eV for KCl, KBr, and KI, respectively; (ii) the lowest conduction-band minimum is located at the Γ point of the Brillouin zone (BZ) and has Γ_6^+ symmetry; (iii) a second minimum in the conduction bands, located roughly 1 eV above the Γ minimum at the X point of the BZ is caused by one of the d bands and has X_7^+ symmetry.

The experimental information which leads to the above conclusions is entirely based on the exciton lines, whereas the band-to-band transitions can hardly be used to construct a band model. This is due to the large number of critical points arising from three valence and at least six conduction bands. On the experimental side, however, there are only a few structures to be explained by this mass of critical points, and, unfortunately, there are no experimental clues as to the location of a certain band-to-band transition. It is, therefore, impossible to assign unambiguously the spectral